Available online at www.sciencedirect.com
ScienceDirect
International Journal of Solids and Structures 44 (2007) 7357–7369
INTERNATIONAL JOURNAL OF SOLIDS AND STRUCTURES
www.elsevier.com/locate/ijsolstr

Interface crack growth for anisotropic plasticity with non-normality effects

Viggo Tvergaard *, Brian Nyvang Legarth

Department of Mechanical Engineering, Solid Mechanics, Technical University of Denmark, DK-2800 Kgs. Lyngby, Denmark

Received 8 January 2007; received in revised form 30 March 2007
Available online 20 April 2007

Abstract

A plasticity model with a non-normality plastic flow rule is used to analyze crack growth along an interface between a solid with plastic anisotropy and an elastic substrate. The fracture process is represented in terms of a traction-separation law specified on the crack plane. A phenomenological elastic–viscoplastic material model is applied, using an anisotropic yield criterion, and in each case analyzed the effect of non-normality is compared with results for the standard normality flow rule. Due to the mismatch of elastic properties across the interface the corresponding elastic solution has an oscillating stress singularity, and with conditions of small scale yielding this solution is applied as boundary conditions on the outer edge of the region analyzed. Crack growth resistance curves are calculated numerically, and the effect of the near-tip mode mixity on the steady-state fracture toughness is determined. It is found that the steady-state fracture toughness is quite sensitive to differences in the initial orientation of the principal axes of the anisotropy relative to the interface.

Keywords: Anisotropic viscoplasticity; Crack growth; Vertex; Finite strains

1. Introduction

Results found by using an abrupt strain path change to determine the shape of the subsequent yield surface in the vicinity of a current loading point (Kuroda and Tvergaard, 1999) have led to the proposal of a vertex-type plastic flow rule on a smooth yield surface for an anisotropic solid (Kuroda and Tvergaard, 2001a). Polycrystal plasticity, using the Taylor model for either f.c.c. or b.c.c. crystal structure, has shown a clear non-normality of the small amount of plastic flow while the stress point moves along the yield surface. This apparent non-normality must be a vertex-type effect resulting from the Taylor model, since normality of each of the slip systems involved is an integral part of the crystal plasticity model (Kuroda and Tvergaard, 1999). Such non-normality has also been found in corresponding experiments for an aluminum alloy and a steel (Kuwabara et al., 2000).

* Corresponding author. Tel.: +45 4525 4273; fax: +45 4593 1475.
E-mail address: viggo@mek.dtu.dk (V. Tvergaard).

0020-7683/$ - see front matter
doi:10.1016/j.ijsolstr.2007.04.014

Crack growth in metals has been modeled in a number of studies by representing the local fracture process in terms of a traction-separation law along the crack plane with a specified work of separation per unit area, while the surrounding material is represented as elastic–plastic (Tvergaard and Hutchinson, 1992, 1993; Tvergaard, 2001). The analyses have shown that plastic work in the material surrounding the crack-tip contributes significantly to the fracture toughness, such that the macroscopic work of fracture is much larger than that of the local fracture process. Recently, this type of analysis has been used to study crack growth along an interface between an anisotropic ductile material and an elastic material that does not yield plastically (Tvergaard and Legarth, to appear). Two anisotropic plasticity models, by Hill (1948) and Barlat et al. (1991), have been applied, using elastic–viscoplastic versions of the material models, so that strain-rate sensitivity was accounted for. As in the previous interface crack growth studies for isotropic plasticity, mixed mode loading was considered and it was found that plastic flow near the crack-tip results in much increased resistance to crack growth when mode II conditions dominate, rather than mode I conditions.

The material model using a vertex-type plastic flow rule on a smooth yield surface for an anisotropic solid (Kuroda and Tvergaard, 2001a) has been recently applied to study crack growth in a homogeneous solid with different rotations of the principal axes of the anisotropy relative to the crack plane (Tvergaard and Legarth, 2006). It was found that at practically all the parameter values considered the non-normality flow rule gives a smaller value of the fracture toughness than that found by using the standard normality flow rule.

In the present paper, the problem of interface crack growth studied in Tvergaard and Legarth (to appear) is reconsidered with the effect of the vertex-type plastic flow rule on a smooth anisotropic yield surface. As in the previous studies, the analyses are carried out for crack growth along an interface between an anisotropic ductile material and an elastic material that does not yield plastically.

2. Material model

The constitutive model with non-normality of the plastic flow rule (Kuroda and Tvergaard, 2001a,b) is used here to analyse interface crack growth under mixed mode I mode II loading. The substrate (see Fig. 1) is taken to be elastic with Young's modulus E_2 and Poissons ratio ν_2 , while material No. 1 above the interface shows anisotropic plasticity, with the elastic properties E_1 and ν_1, and the plane strain analyses are carried out for conditions of small-scale yielding.

The result of the Eulerian kinematics, assuming small elastic and finite plastic deformations, can be expressed by

$$\mathbf{D} = \mathbf{D}^{\mathrm{e}} + \mathbf{D}^{\mathrm{p}} = \mathbf{D}^{\mathrm{e}} + \dot{\Phi}\mathbf{N}^{\mathrm{p}}, \quad \mathbf{W} = \boldsymbol{\omega} + \mathbf{W}^{\mathrm{p}} \tag{2.1}$$

where $\mathbf{D}$ and $\mathbf{W}$ are the symmetric and anti-symmetric parts of the spatial velocity gradient $\mathbf{L} = \partial v_i/\partial x_j\, \mathbf{e}_i \otimes \mathbf{e}_j$ ($\mathbf{v}$ is the velocity of a material particle, $\mathbf{x}$ is the current position and $\mathbf{e}_i$ the Cartesian basis). The superscripts e and p denote elastic and plastic parts, respectively, $\boldsymbol{\omega}$ is the spin of the substructure, and $\mathbf{W}^{\mathrm{p}}$ is the plastic spin.

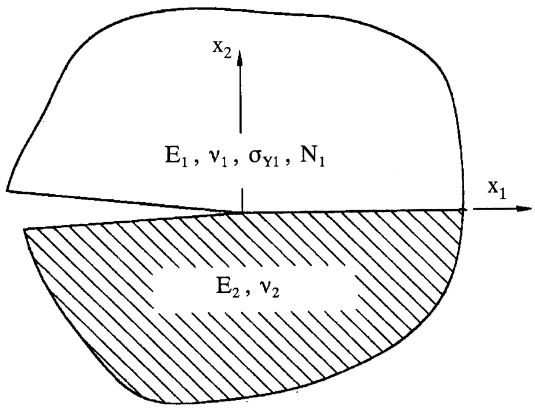

Fig. 1. Interface crack with elastic–plastic material properties above the interface and elastic properties below.

Here it is assumed that $\mathbf{W}^{\mathrm{p}} = \mathbf{0}$, so that $\mathbf{W} = \boldsymbol{\omega}$. The value of the variable $\dot{\Phi}$ is specified below for the rate-dependent case to be considered here.

The elasticity relation is assumed to be given by Hooke's law

$$\overset{\circ}{\boldsymbol{\sigma}} = \dot{\boldsymbol{\sigma}} - \boldsymbol{\omega}\boldsymbol{\sigma} + \boldsymbol{\sigma}\boldsymbol{\omega} = \mathbf{C} : \mathbf{D}^{\mathrm{e}} = \mathbf{C} : \mathbf{D} - \dot{\Phi}\mathbf{C} : \mathbf{N}^{\mathrm{p}} \tag{2.2}$$

where $\boldsymbol{\sigma}$ is the Cauchy stress and $\mathbf{C}$ is a fourth order isotropic elastic moduli tensor, determined by Young's modulus E and Poisson's ratio ν . The superposed o denotes an objective rate with respect to the spin $\boldsymbol{\omega}$ and the superposed dot denotes a material time derivative.

For the anisotropic plasticity representing material No. 1, orthotropic symmetry is assumed. The structure variables to be considered are the orthonormal unit vectors $\mathbf{p}_i$ and the equivalent plastic strain ε^{p}, where $\mathbf{p}_i$ are defined along the axes of orthotropy, $\hat{x}_i$, which evolve according to

$$\dot{\mathbf{p}}_i = \boldsymbol{\omega}\mathbf{p}_i \tag{2.3}$$

since $\overset{\circ}{\mathbf{p}}_i \equiv \mathbf{0}$. The stress components with respect to the orthotropic axes, $\hat{x}_i$, are denoted by $(\hat{})$, so that $\hat{\sigma}_{ij} = \mathbf{p}_i \cdot \boldsymbol{\sigma} \cdot \mathbf{p}_j$ for $i,j = 1,2,3$, see Fig. 2. The initial angle of orientation of plastic anisotropy is denoted by θ_0.

The variable $\dot{\Phi}$ in the flow rule $\mathbf{D}^{\mathrm{p}} = \dot{\Phi}\mathbf{N}^{\mathrm{p}}$ is given by

$$\dot{\Phi} = \dot{\Phi}_0 \left(\frac{K}{g(\varepsilon^{\mathrm{p}})} \right)^{1/m} \tag{2.4}$$

Here $\dot{\Phi}_0$ is a material constant having the dimension of $(\text{time})^{-1}$, m is the strain-rate sensitivity exponent, K is an effective stress value, and ε^{p} is the effective plastic strain defined as

$$\varepsilon^{\mathrm{p}} = \int \dot{\varepsilon}^{p}\, \mathrm{d}t = \int \sqrt{2/3}\dot{\Phi}\, \mathrm{d}t \tag{2.5}$$

The function $g(\varepsilon^{\mathrm{p}})$ in (2.4) represents the effective tensile flow stress in a tensile test in the $\hat{x}_1$ direction, carried out at a strain-rate such that $\dot{\Phi} = \dot{\Phi}_0$ (or $\dot{\varepsilon}^{\mathrm{p}} = \sqrt{2/3}\dot{\Phi}_0$). This function is taken to follow a power law

$$g(\varepsilon^{\mathrm{p}}) = \sigma_{\mathrm{Y1}} \left(1 + \frac{\varepsilon^{\mathrm{p}}}{\varepsilon_0} \right)^{N_1} \tag{2.6}$$

where σ_{Y1} is the initial yield stress, ε_0 is a material constant and N_1 is the strain hardening exponent.

An anisotropic yield condition can be written as

$$f = J(\boldsymbol{\sigma}, \mathbf{p}_i) - K = 0 \tag{2.7}$$

where J is a function of the stress components and the orientation of the axes of orthotropy. In the present rate-dependent formulation the expression $f = 0$ from (2.7) serves as a plastic potential, from which the effective stress value K is determined to be substituted into (2.4).

The material is assumed to be pressure insensitive, i.e. $\partial J/\partial\boldsymbol{\sigma}$ is a deviatoric quantity. The unit outward normal $\mathbf{n}$ to the potential function is given by

$$\mathbf{n} = \left(\frac{\partial J}{\partial \boldsymbol{\sigma}} \right) \Big/ \left\| \frac{\partial J}{\partial \boldsymbol{\sigma}} \right\| \tag{2.8}$$

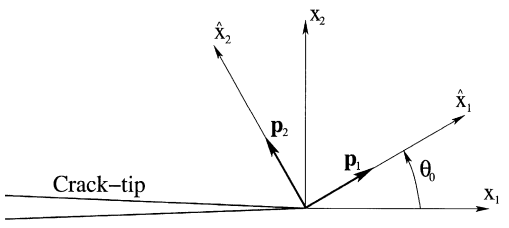

Fig. 2. Definition of the orthonormal basis of plastic anisotropy.

where $\|(\bullet)\| = \sqrt{\mathrm{tr}[(\bullet)^{\mathrm{T}}(\bullet)]}$. An expression for the direction $\mathbf{N}^{\mathrm{p}}$ of the plastic strain rate $\mathbf{D}^{\mathrm{p}}$ is derived in the following manner. Introducing the notation for a deviatoric quantity, $(\bullet)' = (\bullet) - (1/3)(\mathbf{I}\otimes\mathbf{I}):(\bullet)$, with the unity tensor $\mathbf{I}$, a direction $\mathbf{m}$ normal to $\mathbf{n}$ is defined as

$$\mathbf{m} = \frac{\mathbf{D}' - (\mathbf{n}:\mathbf{D}')\mathbf{n}}{\|\mathbf{D}' - (\mathbf{n}:\mathbf{D}')\mathbf{n}\|} \tag{2.9}$$

Then, the direction $\mathbf{N}^{\mathrm{p}}$ of the plastic strain-rate $\mathbf{D}^{\mathrm{p}}$ is taken to be

$$\mathbf{N}^{\mathrm{p}} = \mathbf{n} + \hat{\delta}\mathbf{m} \tag{2.10}$$

where $\hat{\delta}$ is a scalar-valued function to be specified below. Using (2.10) in (2.1), $\mathbf{D}^{\mathrm{p}} = \dot{\Phi}\mathbf{N}^{\mathrm{p}}$ specifies the plasticity model with the vertex-type effect (Simo, 1987), expressing the non-normality of the plastic flow. The value of $\hat{\delta}$ is taken to be given by (Kuroda and Tvergaard, 2001a,b)

$$\hat{\delta} = \tan\varphi^{\mathrm{p}}, \quad \varphi^{\mathrm{p}} = \begin{cases} \alpha\varphi & \text{for } \alpha\varphi \leqslant \varphi^{\mathrm{p}}_{\mathrm{crit}}, \\ \varphi^{\mathrm{p}}_{\mathrm{crit}} & \text{for } \alpha\varphi > \varphi^{\mathrm{p}}_{\mathrm{crit}} \end{cases} \tag{2.11}$$

$$\varphi = \cos^{-1}\left[\frac{\mathbf{n}:\mathbf{D}'}{\|\mathbf{D}'\|}\right], \quad \alpha = \frac{1}{cg/\mu + 1} \tag{2.12}$$

where the coefficient c specifies the degree of noncoaxiality between $\mathbf{D}'$ and $\mathbf{D}^{\mathrm{p}}$, and $\mu = E_1/\{2(1+\nu_1)\}$ is the elastic shear modulus. The ratio μ/g represents the elastic modulus normalised by the current stress level g in (2.6). For usual elastic–viscoplastic materials α is close to unity, but a small deviation from unity has a large effect on predictions of strain localization (Kuroda and Tvergaard, 2001a,b). It is noted that when $\varphi^{\mathrm{p}}_{\mathrm{crit}} \to 0°$ the present flow rule reduces to that of normality.

Plastic anisotropy is here accounted for by using the phenomenological theory proposed by Hill (1948, 1950), which is quadratic in terms of the stress components. Here the expression J in (2.7) is given by

$$J = \sqrt{\frac{1}{G+H}}\left[F(\hat{\sigma}_{22}-\hat{\sigma}_{33})^2 + G(\hat{\sigma}_{33}-\hat{\sigma}_{11})^2 + H(\hat{\sigma}_{11}-\hat{\sigma}_{22})^2 + 2P\hat{\sigma}_{12}^2 + 2L\hat{\sigma}_{23}^2 + 2M\hat{\sigma}_{13}^2\right]^{1/2} \tag{2.13}$$

for $F = G = H = 1$ and $P = L = M = 3$ this expression simplifies to the effective von Mises stress. For plane strain conditions, where $\hat{\sigma}_{13} = \hat{\sigma}_{23} = 0$, the two coefficients of anisotropy M and L are left out of the considerations. The material described by (2.13) is denoted Hill-48 in the following.

For the non-associated model (2.9), in presence of anisotropy, there is the possibility that the plastic work rate is negative, even for $\varphi^{\mathrm{p}}_{\mathrm{crit}} < \pi/2$. The angle $\varphi^{\mathrm{p}}_{\mathrm{crit}}$ should not exceed $\pi/2 - \varphi_{\mathrm{n}\sigma'}$, where $\varphi_{\mathrm{n}\sigma'}$ is the angle between the normal and the stress deviator at the current point on the yield surface. This requirement will be satisfied for moderate intensity of anisotropy and moderate $\varphi^{\mathrm{p}}_{\mathrm{crit}}$. The maximum allowable value of $\varphi^{\mathrm{p}}_{\mathrm{crit}}$ has been calculated numerically to be about 54° for the particular parameter values used here, and thus the applied value $\varphi^{\mathrm{p}}_{\mathrm{crit}} = 20°$ is well within the limits.

3. Cohesive zone at interface

The elastic interface crack problem has been treated by many authors (e.g. England, 1965). Following the formulation of Rice (1988) (see also Tvergaard and Hutchinson, 1993), the crack has tractions acting on the interface which are given by

$$\sigma_{22} + \mathrm{i}\sigma_{12} = (K_{\mathrm{I}} + \mathrm{i}K_{\mathrm{II}})(2\pi r)^{-1/2} r^{\mathrm{i}\varepsilon} \tag{3.1}$$

where K_{I} and K_{II} are the two stress intensity factor components. Here, r is the distance from the tip, $\mathrm{i} = \sqrt{-1}$, ε is the oscillation index

$$\varepsilon = \frac{1}{2\pi}\ln\left(\frac{1-\beta}{1+\beta}\right) \tag{3.2}$$

and β is the second Dundurs' parameter

$$\beta = \frac{1}{2}\frac{\mu_1(1-2\nu_2)-\mu_2(1-2\nu_1)}{\mu_1(1-\nu_2)+\mu_2(1-\nu_1)} \tag{3.3}$$

where the shear moduli are $\mu_1 = E_1/(2(1+\nu_1))$ and $\mu_2 = E_2/(2(1+\nu_2))$. The relation between the energy release rate G and the magnitude $|K|$ of stress intensity factors is

$$G = \frac{1}{2}(1-\beta^2)\left[\frac{1-\nu_1^2}{E_1}+\frac{1-\nu_2^2}{E_2}\right]|K|^2, \quad |K| = \sqrt{K_{\mathrm{I}}^2+K_{\mathrm{II}}^2} \tag{3.4}$$

with a reference length L chosen to characterize the remote field, an L-dependent measure of mode mixity ψ is defined by

$$\tan\psi = \frac{\mathrm{Im}[(K_{\mathrm{I}}+\mathrm{i}K_{\mathrm{II}})L^{\mathrm{i}\varepsilon}]}{\mathrm{Re}[(K_{\mathrm{I}}+\mathrm{i}K_{\mathrm{II}})L^{\mathrm{i}\varepsilon}]} \tag{3.5}$$

which reduces to the more familiar measure, $\tan\psi = K_{\mathrm{II}}/K_{\mathrm{I}}$, when $\varepsilon = 0$. The displacement components associated with the singularity field, with amplitude $|K|$, are specified in (Tvergaard and Hutchinson, 1993).

The x_1-axis is in the crack plane and the initial crack-tip is located at $x_1 = x_2 = 0$ (see Fig. 2). The traction-separation relation used to model the fracture process (Fig. 3) is specified everywhere on the boundary $x_1 > 0$, $x_2 = 0$ of the region analyzed, while zero tractions are specified for $x_1 \leqslant 0$, $x_2 = 0$.

The traction-separation law used by Tvergaard and Hutchinson (1993) is a special version of that proposed by Tvergaard (1990) as a generalization of the model of Needleman (1987). Here, δ_{n} and δ_{t} denote the normal and tangential components of the relative displacement of the crack faces across the interface in the zone where the fracture processes are occurring (Fig. 3). When $\delta_{\mathrm{n}}^{\mathrm{c}}$ and $\delta_{\mathrm{t}}^{\mathrm{c}}$ are critical values of these displacement components and a single non-dimensional separation measure is defined as $\lambda = [(\delta_{\mathrm{n}}/\delta_{\mathrm{n}}^{\mathrm{c}})^2 + (\delta_{\mathrm{t}}/\delta_{\mathrm{t}}^{\mathrm{c}})^2]^{1/2}$ the tractions drop to zero when $\lambda = 1$. With $\sigma(\lambda)$ displayed in Fig. 3, a potential from which the tractions are derived is defined as

$$\Phi^*(\delta_{\mathrm{n}},\delta_{\mathrm{t}}) = \delta_{\mathrm{n}}^{\mathrm{c}}\int_0^{\lambda}\sigma(\lambda')\,\mathrm{d}\lambda' \tag{3.6}$$

The normal and tangential components of the traction acting on the interface in the fracture process zone are given by

$$T_{\mathrm{n}} = \frac{\partial\Phi^*}{\partial\delta_{\mathrm{n}}} = \frac{\sigma(\lambda)}{\lambda}\frac{\delta_{\mathrm{n}}}{\delta_{\mathrm{n}}^{\mathrm{c}}}, \quad T_{\mathrm{t}} = \frac{\partial\Phi^*}{\partial\delta_{\mathrm{t}}} = \frac{\sigma(\lambda)}{\lambda}\frac{\delta_{\mathrm{t}}}{\delta_{\mathrm{t}}^{\mathrm{c}}}\frac{\delta_{\mathrm{n}}^{\mathrm{c}}}{\delta_{\mathrm{t}}^{\mathrm{c}}} \tag{3.7}$$

The peak normal traction under pure normal separation is $\hat{\sigma}$, and the peak shear traction is $(\delta_{\mathrm{n}}^{\mathrm{c}}/\delta_{\mathrm{t}}^{\mathrm{c}})\hat{\sigma}$ in a pure tangential separation. The work of separation per unit area of interface is given by Eq. (3.6) with $\lambda = 1$, and for the separation function $\sigma(\lambda)$ in Fig. 3 the work is

$$\Gamma_0 = \frac{1}{2}\hat{\sigma}\delta_{\mathrm{n}}^{\mathrm{c}}(1-\lambda_1+\lambda_2) \tag{3.8}$$

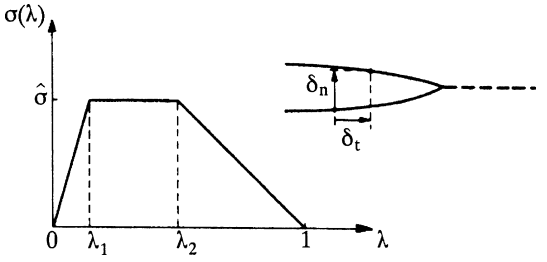

Fig. 3. Specification of traction-separation relation.

It has been found in (Tvergaard and Hutchinson, 1992, 1993) that the two most important parameters characterizing the fracture process in this model are Γ_0 and $\hat{\sigma}$. Scheider and Brocks (2003) have found cases where also differences in the shape of the separation law have an important effect.

Based on (3.4) and (3.8) a reference stress intensity factor is defined as

$$K_0 = \left[\frac{1-\nu_1^2}{E_1}+\frac{1-\nu_2^2}{E_2}\right]^{-1/2}\left(\frac{2\Gamma_0}{1-\beta^2}\right)^{1/2} \tag{3.9}$$

here, K_0 represents the value of $|K|$ needed to advance the interface crack in the absence of any plasticity. This value is independent of ψ since a potential is used to generate the relation of tractions to crack face displacements of the interface. A length quantity R_0, which scales with the size of the plastic zone in material No. 1 (when $|K| \cong K_0$), is defined by

$$R_0 = \frac{1}{3\pi}\left(\frac{K_0}{\sigma_{Y1}}\right)^2 = \frac{2}{3\pi}\left[\frac{1-\nu_1^2}{E_1}+\frac{1-\nu_2^2}{E_2}\right]^{-1}\frac{\Gamma_0}{(1-\beta^2)\sigma_{Y1}^2} \tag{3.10}$$

While the mode mixity measure ψ refers to the distance L from the tip, it is natural to define a reference measure of mixity, ψ_0, based on the reference length R_0. The relation between ψ_0 and ψ is

$$\psi_0 = \psi + \varepsilon \ln(R_0/L) \tag{3.11}$$

4. Numerical method

The numerical crack growth procedure follows that of Tvergaard and Legarth (2004). Thus, the finite-element approximation of the displacement fields is used in the context of an updated Lagrangian formulation (McMeeking and Rice, 1975) based on the principle of virtual work. The incremental form of the principle of virtual work in terms of the 1st Piola–Kirchhoff stress, $s_{ij} \neq s_{ji}$, is (Yamada and Hirakawa, 1978; Tvergaard, 1990; Yamada and Sasaki, 1995)

$$\begin{aligned}
&\Delta t\int_V \dot{s}_{ij}\delta v_{j,i}\,\mathrm{d}V + \Delta t\int_{S_\mathrm{I}}\{\dot{T}_\mathrm{n}\delta(\dot{\delta}_\mathrm{n})+\dot{T}_\mathrm{t}\delta(\dot{\delta}_\mathrm{t})\}\,\mathrm{d}S = \Delta t\int_S \dot{T}_i\delta v_i\,\mathrm{d}S \\
&\quad -\left[\int_V s_{ij}\delta v_{j,i}\,\mathrm{d}V - \int_S T_i\delta v_i\,\mathrm{d}S + \int_{S_\mathrm{I}}\{T_\mathrm{n}\delta(\dot{\delta}_\mathrm{n})+T_\mathrm{t}\delta(\dot{\delta}_\mathrm{t})\}\,\mathrm{d}S\right] \\
&T_i = s_{ji}n_j
\end{aligned} \tag{4.1}$$

where V is the volume, S is the surface and S_I denotes the debonding interface, T_i are the nominal tractions and δv_i are the virtual velocities in the current deformed configuration. Therefore, in the updated Lagrangian formulation s_{ij} is identical to σ_{ij} before the increment, but $\dot{s}_{ij}$ is not equal to $\dot{\sigma}_{ij}$, i.e. $\dot{\mathbf{s}} = \dot{\boldsymbol{\sigma}} - \mathbf{L}\boldsymbol{\sigma} + \mathrm{tr}(\mathbf{L})\boldsymbol{\sigma}$. The bracketed terms in Eq. (4.1) are equilibrium correction terms.

An example of the mesh used for the computations is shown in Fig. 4, where it is seen that a uniform mesh region is used in the range where crack growth is studied. The length of one square element inside the uniform mesh is denoted Δ_0, and the initial crack tip is located at $x^1 = 0$. The computations are carried out with 120×6 quadrilaterals in the uniform mesh along the interface. The elements used are quadrilaterals each built-up of four triangular, linear displacement elements. The outer radius of the region analysed is chosen to be $A_0/\Delta_0 = 800{,}000$, in order that the plastic zone size should not exceed $A_0/10$.

During the initial part of the crack growth resistance curve an increment of $|K|$ is prescribed, but when $|K|$ approaches its asymptote, a Rayleigh–Ritz finite-element method (Tvergaard, 1976) is needed to ensure that the crack keeps growing, even though the value of $|K|$ may decrease slightly. Thus, at the point of the crack surface, where the displacement difference across the crack has increased most in the previous increment, the displacement difference is prescribed to keep increasing. It is noted that full finite strain effects are accounted for so that crack-tip blunting can be represented, and this is important if the peak stress $\hat{\sigma}$ of the debonding model is near or above the maximum possible stress during blunting, as discussed by Tvergaard and Hutchinson (1992). In each increment the time step, Δt, for the next increment is corrected according to

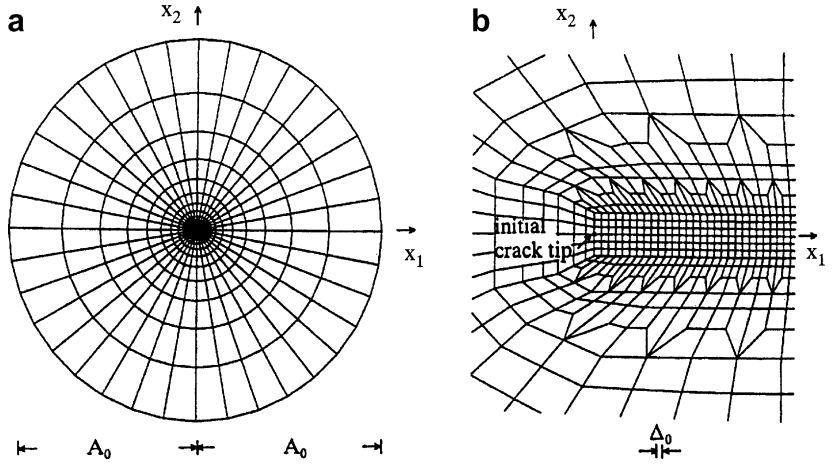

Fig. 4. Mesh used for some of the crack growth analyses.

$(\dot{\varepsilon}^{\mathrm{p}})_{\max}\cdot\Delta t\leqslant c_1$ and $(\dot{\lambda})_{\max}\cdot\Delta t\leqslant c_2$, where the label max refers to the maximum effective plastic strain rate in any triangular element, or the maximum rate of the debonding separation measure λ, at the current increment. The values of the constants c_1 and c_2 are in several computations chosen as $c_1=0.02$ and $c_2=0.004$, but in some cases smaller values of the constants have been needed, to avoid numerical instabilities.

5. Results

The plastically anisotropic metal represented here as material No. 1 above the interface (see Fig. 1) is an aluminium alloy Al 7108-T7, for which Moen et al. (1998) (see also Legarth et al., 2002) used a fitting in terms of Hill-48. In the yield function (2.13) the parameter values are

$$F=0.699,\quad G=3.33,\quad H=1,\quad P=9.60 \tag{5.1}$$

Additional material parameters, used to fit a uniaxial tensile test with only $\sigma_{11}\neq 0$, are $\sigma_{\mathrm{Y1}}/E_1=0.003$, $\varepsilon_0=0.005$, $\nu_1=0.3$, $N_1=0.1$, $m=0.005$ and $\dot{\Phi}_0=0.002\,\mathrm{s}^{-1}$. In the traction-separation law the values $\delta_{\mathrm{n}}^{\mathrm{c}}/\delta_{\mathrm{t}}^{\mathrm{c}}=1$, $\delta_{\mathrm{n}}^{\mathrm{c}}=0.1\Delta_0$, $\lambda_1=0.15$ and $\lambda_2=0.50$ are used, while $\hat{\sigma}/\sigma_{\mathrm{Y1}}$ is varied. In the analyses to be presented here, with $\nu_2=\nu_1$, it will be assumed that the substrate (Fig. 1) has a higher elastic stiffness, such that $E_2/E_1=6$, and does not yield plastically.

Uniaxial plane strain tension in the x_1-direction has been used (Tvergaard and Legarth, 2004) to illustrate the variation of the plane strain yield stress with the initial angle of anisotropy orientation, θ_0, relative to the x_1-direction. The lowest yield stress was found for $\theta_0=45°$, below the isotropic yield stress, while the yield stress near $\theta_0=0°$ and $\theta_0=90°$ was above the isotropic yield stress.

Crack growth resistance curves have been calculated for different values of the material parameters, and for several values of the initial angle θ_0 between the x_1 axis and the principal axis of the anisotropy. Fig. 5 shows examples of the calculated resistance curves for the Hill-48 material, for $\hat{\sigma}/\sigma_{\mathrm{Y1}}=2.5$ and the values 45° or 135° of the initial angle of inclination, θ_0, of the anisotropy, with the mode mixity near the crack-tip specified by $\psi_0=3.52°$. These curves are compared with corresponding curves for the Mises material, and in all cases the crack growth resistance curves have been calculated for the materials with the normality flow rule, as well as for non-normality with $c=2$ and $\varphi_{\mathrm{crit}}^{\mathrm{p}}=20°$. The $|K|$-axis is normalised by the reference value K_0 in (3.9) and the amount of crack growth Δa is normalised by the reference length R_0 in (3.10).

In all cases in Fig. 5 it is seen that crack growth initiates at $|K|=K_0$. The resistance curves for the Hill-48 material as well as those for the Mises material show that the maximum levels of fracture toughness are reduced when the non-normality flow rule is applied. Furthermore, the curves for the Mises materials have lower maxima than those for Hill-48. Also, the maxima occur at significantly larger values of $\Delta a/R_o$ for the anisotropic materials than for isotropic plasticity.

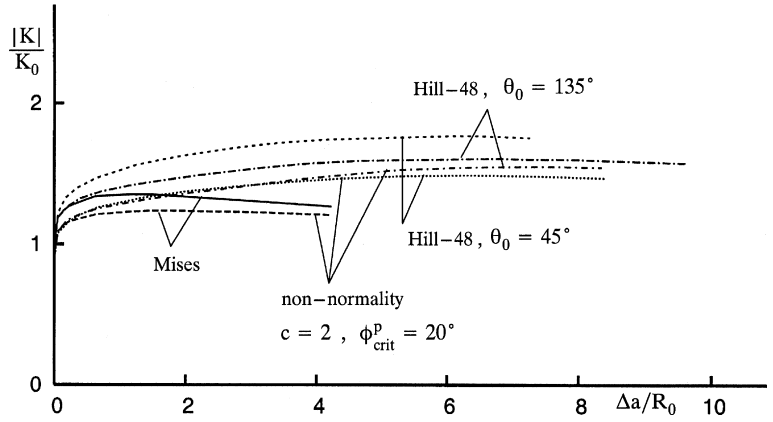

Fig. 5. Interface crack growth resistance curves for $\hat{\sigma}/\sigma_{Y1} = 2.5$ and two different values of the initial angle of inclination θ_0 of the anisotropy. Curves for the non-normality flow rule are compared with the results for normality, and results for the Mises yield condition are also shown. The near-tip mode mixity is specified by $\psi_0 = 3.52°$.

Similar resistance curves are shown in Fig. 6 for $\theta_0 = 0°$ and $\theta_0 = 90°$, again compared with the corresponding Mises materials. Here, the curves for the two different orientations of the Hill-48 material differ a great deal, and the lower toughnesses, for $\theta_0 = 0°$ are of the same order of magnitude as those found for the Mises materials. The maxima of the curves for $\theta_0 = 90°$ are only a little below those found for other values of θ_0 in Fig. 5, but the maxima occur at smaller values of $\Delta a/R_o$.

In the initial parts of the resistance curves for the elastic–viscoplastic materials considered the rate of increase of the stress intensity factor $|K|$ is taken to be $|\dot{K}| = K_0/t_R$, where t_R is a reference time. When the resistance curve flattens out, approaching the maximum value of $|K|$, the value of $|\dot{K}|$ will have to approach zero, so that a positive value of $|\dot{K}|$ cannot be specified. Instead, the rate of crack growth is specified such that the rate of crack opening at the crack-tip is $\dot{\delta}_n = \delta_n^c/t_R$. In most of the analyses the value of the reference time is chosen as $t_R = 0.2/\dot{\varepsilon}_0$, but the calculated resistance curves will show some dependence on the rate of loading, since the material is described as elastic–viscoplastic. To quantify this rate-dependence, one of the curves from Fig. 5 (for Hill-48, $\theta_0 = 45°$, $c = 2$ and $\varphi^p_{crit} = 20°$) has been recomputed with a ten times larger and a ten times smaller value of t_R, as shown in Fig. 7. For the ten times larger value of t_R the rate of crack growth is ten times smaller, and the smaller strain rates give lower stress levels in the viscoplastic material. But it is seen in Fig. 7, for the low value of the rate-hardening exponent m applied here, that the sensitivity to the value of t_R is quite small.

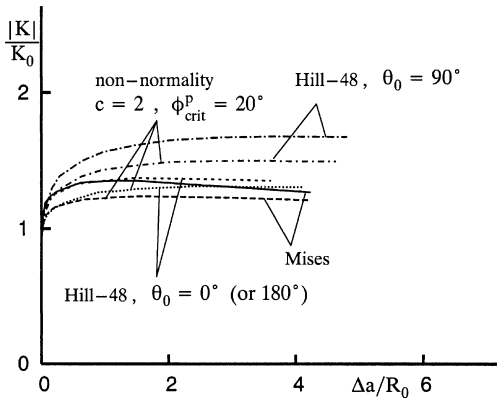

Fig. 6. Interface crack growth resistance curves for $\hat{\sigma}/\sigma_{Y1} = 2.5$ and two different values of the initial angle of inclination θ_0 of the anisotropy. Curves for the non-normality flow rule are compared with the results for normality, and results for the Mises yield condition are also shown. The near-tip mode mixity is specified by $\psi_0 = 3.52°$.

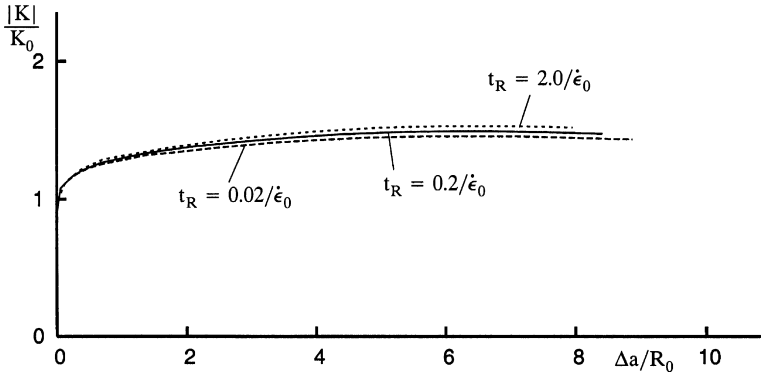

Fig. 7. Interface crack growth resistance curves for three different values of the loading rate, as specified by the reference time t_R, where $|\dot{K}| = K_0/t_R$ or $\dot{\delta}_n = \delta_n^c/t_R$. Here, the non-normality flow rule is applied, for $\theta_0 = 45°$, $\hat{\sigma}/\sigma_{Y1} = 2.5$ and $\psi_0 = 3.52°$.

A limiting value of $|K|$, to be denoted $|K|_{ss}$, is attained as the crack grows and approaches a steady-state. Some of the predicted resistance curves go slightly downwards after reaching the maximum, so that $|K|_{ss}$ is approached from above, as has been discussed by Tvergaard and Hutchinson (1993), but in these cases the values $|K|_{ss}$ are here identified as the peak values of the resistance curves.

In Fig. 8 the variation of the steady-state values $|K|_{ss}/K_0$ with the mode mixity parameter ψ_0 is plotted for six different cases, corresponding to the resistance curves shown in Fig. 5, i.e. for the Hill-48 material, with $\hat{\sigma}/\sigma_{Y1} = 2.5$ and the values 45° or 135° of the initial angle of inclination, θ_0, of the anisotropy relative to the interface. In Fig. 5, for $\psi_0 = 3.52°$, the peak values of the two curves for $\theta_0 = 135°$ are in between the peak values of the two curves for $\theta_0 = 45°$, but Fig. 8 shows that the two curves for non-normality intersect at a negative value of ψ_0 . In all of the range considered the two curves for the Mises materials are below the corresponding curves for the Hill-48 materials, and all three curves accounting for non-normality are below the corresponding curves calculated for $\varphi_{crit}^p = 0°$. All six curves in Fig. 8 have minima in the near vicinity of $\psi_0 \approx 0°$, where the conditions near the crack-tip are close to pure mode I.

For $\theta_0 = 0°$ and $\theta_0 = 90°$ curves of the steady-state value $|K|_{ss}/K_0$ versus the mode mixity parameter ψ_0 are plotted in Fig. 9, including the peak values of the resistance curves in Fig. 6 for $\psi_0 = 3.52°$. The relative levels of the peak values for the different cases found in Fig. 6 are not maintained in the whole range of Fig. 9, as a

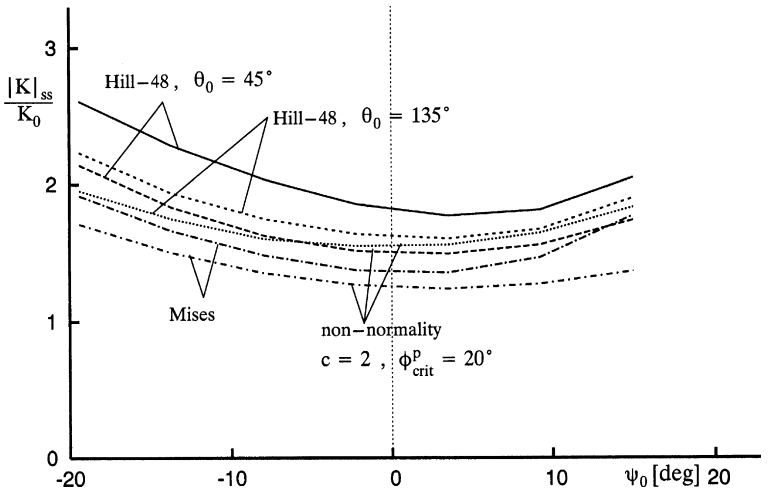

Fig. 8. Steady-state interface toughness as a function of the local mixity measure ψ_0 for $\hat{\sigma}/\sigma_{Y1} = 2.5$, and for two different values of the initial angle of inclination θ_0 of the anisotropy. Curves for the non-normality flow rule are compared with the results for normality, and results for the Mises yield condition are also shown.

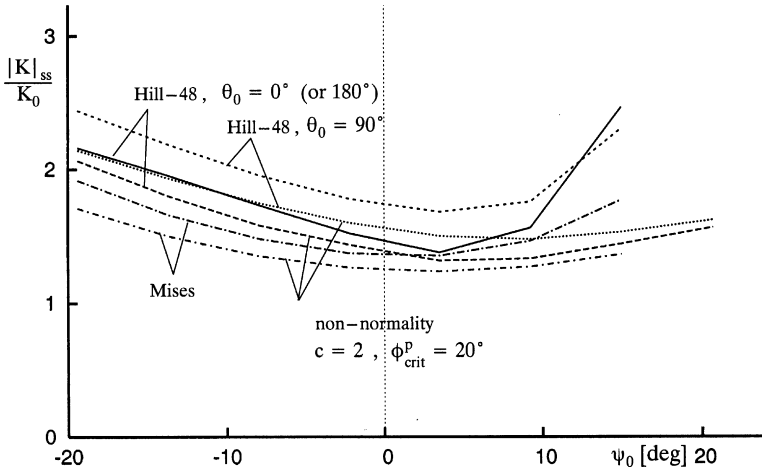

Fig. 9. Steady-state interface toughness as a function of the local mixity measure ψ_0 for $\hat{\sigma}/\sigma_{Y1} = 2.5$, and for two different values of the initial angle of inclination θ_0 of the anisotropy. Curves for the non-normality flow rule are compared with the results for normality, and results for the Mises yield condition are also shown.

number of the curves intersect. However, the three curves accounting for non-normality are all below the corresponding curves calculated for $\varphi^{p}_{crit} = 0°$. At positive values of ψ_0 these three curves show little dependence on increasing mode mixity, whereas the three curves for $\varphi^{p}_{crit} = 0°$ show a steep increase of the fracture toughness as the value of ψ_0 increases.

For $\theta_0 = 45°$ the influence of different values of the peak stress, $\hat{\sigma}$, in the traction-separation law for the interface is studied in Fig. 10, still considering the steady-state value $|K|_{ss}/K_0$ versus the mode mixity parameter ψ_0. For the low value, $\hat{\sigma}/\sigma_{Y1} = 1.25$, the characteristic feature is illustrated (see also Tvergaard and Hutchinson, 1993) that the fracture toughness is constant, $|K|_{ss}/K_0 \approx 1.0$, in a rather wide range around $\psi_0 \approx 0°$, where crack growth is not affected by plasticity. Also for $\hat{\sigma}/\sigma_{Y1} = 1.5$ there is a central range of nearly constant fracture toughness, whereas such a range is not seen for $\hat{\sigma}/\sigma_{Y1} = 2.5$ (this curve was also shown in Fig. 8). Three of the curves in Fig. 10 are predictions based on non-normality, but for $\hat{\sigma}/\sigma_{Y1} = 1.5$ the curve calculated for $\varphi^{p}_{crit} = 0^{\circ}$ is included, again showing that this gives higher toughness in the range affected by plasticity.

In Fig. 11 the dependence of the steady-state interface toughness on the value of the peak stress $\hat{\sigma}/\sigma_{Y1}$ is studied for values of ψ_0 that range from 1.6° at the lowest value of $\hat{\sigma}/\sigma_{Y1}$ to 4.5° at the highest value. The curves compared are calculated for $\theta_0 = 45°$ and for $\theta_0 = 135°$, thus relating to the results displayed in Figs. 5, 8 and 10 for Hill-48. Generally, the curves obtained by the non-normality model are below those for normality, but in the case of $\theta_0 = 135°$ there is a range for $\hat{\sigma}/\sigma_{Y1} < 2.3$, where the trend is opposite but the dif-

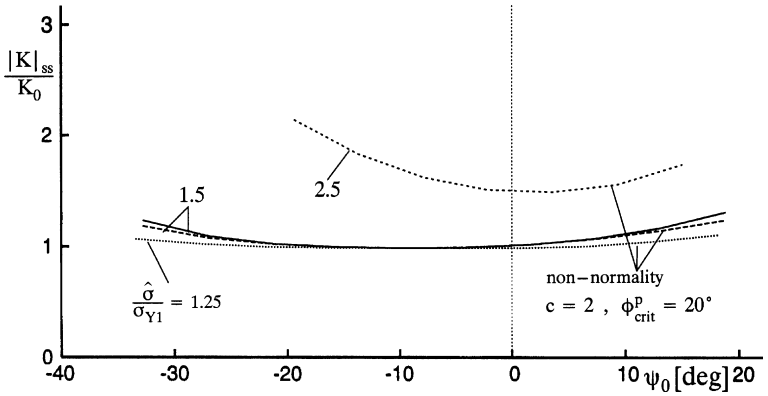

Fig. 10. Steady-state interface toughness as a function of the local mixity measure ψ_0 for three different values of $\hat{\sigma}/\sigma_{Y1}$, and for $\theta_0 = 45°$.

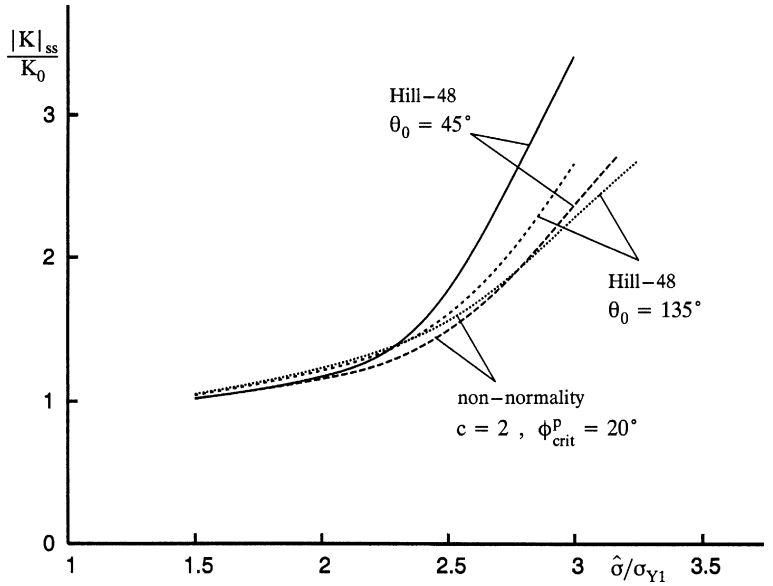

Fig. 11. Steady-state interface toughness vs. peak stress in the cohesive zone model. The values of ψ_0 range from 1.6° at the lowest value of $\hat{\sigma}/\sigma_{Y1}$ to 4.5° at the highest value. Two different values of the initial angle of inclination θ_0 of the anisotropy are considered, for the non-normality flow rule as well as for standard normality.

ference is very small. Fig. 12 shows similar curves for $\theta_0 = 0°$ and $\theta_0 = 90°$, relating to the results displayed in Figs. 6 and 9. As in the previous figure the fracture toughness increases rapidly for increasing value of $\hat{\sigma}/\sigma_{Y1}$, and the curves show significant sensitivity to the value of θ_0.

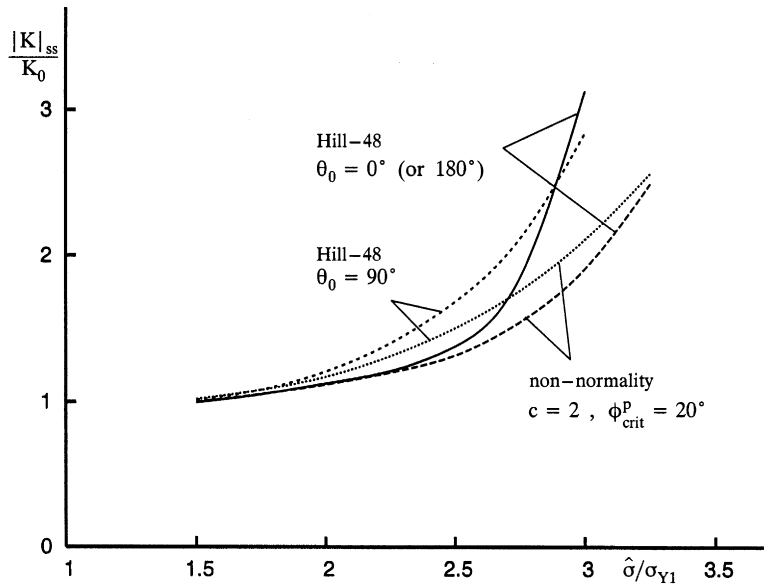

Fig. 12. Steady-state interface toughness vs. peak stress in the cohesive zone model. The values of ψ_0 range from 1.6° at the lowest value of $\hat{\sigma}/\sigma_{Y1}$ to 4.5° at the highest value. Two different values of the initial angle of inclination θ_0 of the anisotropy are considered, for the non-normality flow rule as well as for standard normality.

6. Discussion

A vertex on the yield surface, such as that represented by J_2 corner theory (Christoffersen and Hutchinson, 1979), results in a reduced resistance to non-proportional stress history, as is found for polycrystal plasticity. The same type of effect is represented by the non-normality flow rule for an anisotropic solid, as has been shown by Kuroda and Tvergaard (2001a,b). Therefore, a significant effect of the vertex-type plastic flow rule is expected in crack growth predictions, where the stress history is not proportional. In the present paper the focus is on a metal-ceramic system, where a crack grows along the interface between an aluminium and a ceramic and the interest is in the possibility that the aluminium shows a vertex-type response. Experimental studies, in which yield surfaces are determined by following stress paths in different radial directions do usually not show clear evidence of a vertex. However, Hecker (1976) has studied the existence of a corner on yield surfaces, based on experiments using zig–zag loading, and has found indications of a corner for several materials. The previous study for crack growth under mode I conditions in a homogeneous anisotropic solid (Tvergaard and Legarth, 2006) has shown that the fracture toughness predicted by the non-normality model is much reduced relative to that obtained by the standard normality flow rule. The same general result is found here for crack growth along an interface between an anisotropic elastic–plastic solid and an elastic substrate, for a wide range of mixed-mode loading on the crack-tip.

Although yield surface measurements frequently show no evidence of a vertex, there is much indirect evidence in results for plastic instabilities, where predictions based on the normality rule for a smooth yield surface often give a poor approximation, or fail to predict the instabilities that have been observed experimentally. This is well-known in plastic buckling of plate and shell structures, as has been discussed by Hutchinson (1974), and is also found for localized necking in biaxially stretched metal sheets (Støren and Rice, 1975) or for shear band instabilities in a plane strain tensile test (Tvergaard et al., 1981).

The predicted steady-state fracture toughness $|K|_{ss}/K_0$ is very sensitive to the value of the peak stress in the cohesive zone model, i.e. to the value of the ratio $\hat{\sigma}/\sigma_{Y1}$, as has been found in a number of previous investigations using a cohesive zone to model crack growth in a ductile solid. Also, in agreement with earlier studies of interface crack growth, for different material systems, it is found here that for a given interface strength the fracture toughness is lowest when the value of the mode-mixity parameter ψ_0 is somewhere in the near vicinity of zero, i.e. near mode 1 conditions at the crack-tip. The flat part of the lower curve in Fig. 10 illustrates that the fracture toughness depends only on the local work of separation Γ_0 on the crack plane, when $\hat{\sigma}/\sigma_{Y1}$ is small enough so that plasticity at the crack-tip plays only a minor role. Since the inelastic material above the interface is described as elastic–viscoplastic, while the traction-separation law for the interface is independent of the rate of deformation, the predicted fracture toughnesses will show some dependence on the rate of loading, but the crack growth resistance curves in Fig. 7 illustrate that this dependence is weak in the present cases, where the value of the rate-hardening exponent is small, $m = 0.005$.

The anisotropic material considered here is an aluminium alloy, which is approximated in terms of the Hill-48 yield criterion. In previous studies for crack growth in anisotropic solids the present authors have also considered materials approximated by the yield criterion Barlat et al. (1991), but similar features are found for both models of anisotropy, and therefore only one has been considered here.

The results in Figs. 5, 6, 8 and 9 confirm that the initial orientation of the principal axes of the anisotropy, as specified by the value of the angle θ_0, has a significant influence on the fracture toughness, as was also found in the previous study of interface crack growth (Tvergaard and Legarth, to appear). Also the amount of crack growth needed to reach the maximum fracture toughness varies a great deal as a function of θ_0. Furthermore, it is clear from these figures, and from Figs. 11 and 12, that the effect of the non-normality flow rule is to reduce the fracture toughness in all the cases analysed.

It is important to mention here that the analyses are based on the assumption that the growing crack remains on the interface. In a real material system the crack could grow away from the initial crack plane, but the assumption here is that the interface bonding is weaker than the most weak directions in the anisotropic solid, so that crack growth will not deviate from the interface. Other numerical techniques can be used to study crack growth along a path deviating from the interface (Rashid and Tvergaard, 2003, 2004), but then a fracture criterion has to be established for the anisotropic metal, defining the fracture strength along different orientations of a crack path.

7. Conclusions

Plastic anisotropy is frequently found in structural metals, due to texture or due to the microstructure. This means that the stress levels during plastic flow depend strongly on the orientation of the anisotropy. As a consequence the present analyses show that the resistance to interface crack growth is very sensitive to the orientation of the principal axes of the anisotropy relative to the interface.

A number of structural metals show a vertex-type response during plastic flow. It has been found here that the interface crack growth resistance will be reduced for such materials.

References

Barlat, F., Lege, D.J., Brem, J.C., 1991. A six-component yield function for anisotropic materials. Int. J. Plast. 7, 693–712.

Christoffersen, J., Hutchinson, J.W., 1979. A class of phenomenological corner theories of plasticity. J. Mech. Phys. Solids 27, 465–487.

England, A.H., 1965. A crack between dissimilar media. J. Appl. Mech. 32, 400–402.

Hecker, S.S., 1976. Experimental studies of yield phenomena in biaxially loaded metals. Constitutive Equations in Viscoplasticity. Computational and Engineering Aspects, ASME New York, pp. 1–33.

Hill, R., 1948. A theory of the yielding and plastic flow anisotropic metals. Proceedings of the Royal Society of London A 193, 281–297.

Hill, R., 1950. The Mathematical Theory of Plasticity. The Clarendon Press, Oxford.

Hutchinson, J.W., 1974. Plastic buckling. Adv. Appl. Mech. 14, 67–144.

Kuroda, M., Tvergaard, V., 1999. Use of abrupt strain path change for determining subsequent yield surface: illustrations of basic idea. Acta Mater. 47, 3879–3890.

Kuroda, M., Tvergaard, V., 2001a. A phenomenological plasticity model with non-normality effects representing observations in crystal plasticity. J. Mech. Phys. Solids 49, 1239–1263.

Kuroda, M., Tvergaard, V., 2001b. Shear band development predicted by a non-normality theory of plasticity and comparison to crystal plasticity. Int. J. Solids Struct. 38, 8945–8960.

Kuwabara, T., Kuroda, M., Tvergaard, V., Nomura, K., 2000. Use of abrupt strain path change for determining subsequent yield surface: experimental study with metal sheets. Acta Mater. 48, 2071–2079.

Legarth, B.N., Tvergaard, V., Kuroda, M., 2002. Effects of plastic anisotropy on crack-tip behaviour. Int. J. Fracture 117, 297–312.

McMeeking, R.M., Rice, J.R., 1975. Finite-element formulations for problems of large elastic–plastic deformation. Int. J. Solids Struct. 11, 601–616.

Moen, L.A., Langseth, M., Hopperstad, O., 1998. Elastoplastic buckling of anisotropic aluminum plate elements. J. Struct. Engin., 712–719.

Needleman, A., 1987. A continuum model for void nucleation by inclusion debonding. J. Appl. Mech. 54, 525–531.

Rashid, M.M., Tvergaard, V., 2003. On the path of a crack near a graded interface under large scale yielding. Int. J. Solids Struct. 40, 2819–2831.

Rashid, M.M., Tvergaard, V., 2004. Effect of a graded interface on a crack approaching at an oblique angle. Int. J. Comp. Engin. Sci. 5, 781–794.

Rice, J.R., 1988. Elastic fracture mechanics concepts for interfacial cracks. J. Appl. Mech. 55, 98–103.

Scheider, I., Brocks, W., 2003. The effect of the traction separation law on the results for cohesive zone crack propagation analyses. Key Engin. Mater., 313–318.

Simo, J.C., 1987. A J_2-flow theory exhibiting a corner-like effect and suitable for large-scale computation. Comput. Methods Appl. Mech. Engin. 62, 169–194.

Støren, S., Rice, J.R., 1975. Localized necking in thin sheets. J. Mech. Phys. Solids 23, 421–441.

Tvergaard, V., 1976. Effect of thickness inhomogeneities in internally pressurized elastic-plastic spherical shells. J. Mech. Phys. Solids 24, 291–304.

Tvergaard, V., 1990. Effect of fibre debonding in a whisker-reinforced metal. Mater. Sci. Engin. A125, 203–213.

Tvergaard, V., 2001. Resistance curves for mixed mode interface crack growth between dissimilar elastic–plastic solids. J. Mech. Phys. Solids 49, 2689–2703.

Tvergaard, V., Needleman, A., Lo, K.K., 1981. Flow localization in the plane strain tensile test. J. Mech. Phys. Solids 29, 115–142.

Tvergaard, V., Hutchinson, J.W., 1992. The relation between crack growth resistance and fracture process parameters in elastic–plastic solids. J. Mech. Phys. Solids 40, 1377–1397.

Tvergaard, V., Hutchinson, J.W., 1993. The influence of plasticity on mixed mode interface toughness. J. Mech. Phys. Solids 41, 1119–1135.

Tvergaard, V., Legarth, B.N., 2004. Effect of plastic anisotropy on crack growth resistance under mode 1 loading. Int. J. Fracture 130, 411–425.

Tvergaard, V., Legarth, B.N., 2006. Crack growth resistance for anisotropic plasticity with non-normality effects. Int. J. Solids Struct. 43, 2160–2173.

Tvergaard, V., Legarth, B.N. (to appear). Effect of anisotropic plasticity on mixed mode interface crack growth. Engin. Fracture Mech.

Yamada, Y., Hirakawa, H., 1978. Large deformation and instability analysis in metal forming process. Appl. Numer. Methods Forming Process., ASME, AMD 28, 27–38.

Yamada, Y., Sasaki, M., 1995. Elastic–plastic large deformation analysis program and lamina compression test. Int. J. Mech., 691–707.